A High Resolution and Precision Broad Band Radar

Tomoo Ushio, T. Mega, T. Morimoto, Z-I. Kawasaki, and K. Okamoto
Osaka University, Osaka, Japan

INTRODUCTION

Rainfall observations using weather radar have the major advantage that it is possible to observe precipitation widely in a short time. However, the rain rate obtained by weather radar does not necessarily correspond to that observed by ground based rain gauges. One of the causes of this disagreement is the non-uniformity distribution of raindrops in a rain scattering volume. Another cause is that most types of radar cannot obtain a rain echo at low altitude, because the radar beam overshoots by several kilometers in height due to the earth's curvature, or in vertical pointing mode the receiver is turned off while the pulse is being transmitted. Therefore, to identify how the reflectivity profile changes near the ground and to estimate precisely the causes of the reflectivity measurement errors, a radar capable of observing the reflectivity from near the ground with high resolution and high precision is needed. In addition, our interest in the fine structure of the bright band, or melting layer, which is important for constructing the algorithm of space-borne microwave radiometers, motivated us to develop a high resolution radar.

In this study, we developed a bistatic Ku-band broad band radar(BBR) which can transmit and receive wide band (80 MHz) signals, to obtain good estimates of the radar reflectivity factor at low altitude with high range resolution. The radar uses the pulse compression technique, which transmits a long modulated pulse and then compresses the received signal with a matched filter. Using this technique, we can acquire rainfall profiles of high range resolution and high SNR. The results show that the developed radar can observe the reflectivity profile from 40 m to several km by 100 mW transmitting power.

DESCRIPTION OF THE BROAD BAND RADAR

A. Configuration

In this study, we developed a bistatic high resolution and low power radar system using a wide band signal for the transmitting and pulse compression technique. The pulse compression technique has the advantage that high range resolution profiles can be acquired by low transmitted power. However, the range side lobe of a compressed signal may contaminate the neighboring rain echo. To overcome this disadvantage, we adopted an arbitrary waveform generator (AWG) for the signal source of our radar system and directly acquired the IF signal by a high-speed A/D converter. We can thus flexibly choose any transmitted waveform which results in low side lobe by digital pulse compression. In this study, we used the chirp signal with the Blackman-Harris and

raised-cosine window function for suppressing the range sidelobe.

In figure 1, a schematic diagram of the radar system is shown. This system consists of transmitting and receiving Cassegrain type antennas, transceiver, AWG, A/D converter and GPS receiver. The diameters of the antennas are 60 cm. The chirp signal of the 20−100 MHz frequency range in the pulse width of 128 μs is generated by the AWG. The double phase lock oscillators in the transceiver up-convert this output to 15.71−15.79 GHz, and this output is amplified by a solid state amplifier to about 100 mW.

The echo received from precipitation is down-converted to an IF signal in the transceiver. The signal is sampled by the A/D converter (sampling ratio: 400 Msamples/s, bit rate: 12 bits/sample, available memory: 4 Msamples) and is saved to the PC. The high-precision 10-MHz reference clock from the GPS receiver synchronizes the internal clock of the AWG and the A/D converter. The GPS is also used for time synchronizing the other equipment such as the disdrometer.

B. Signal Processing Procedure

In this radar system, we take the pulse compression approach to have the reflectivitiess. In the pulse compression processing, we calculate the cross-correlation between the signal received from precipitation and the reference signal. The reference signal is pre-sampled by directly connecting the transceiver output of the transmitting end to the input of the receiving end through the attenuator. In the cross-correlation, we use FFT in the frequency domain, and multiply the received signal with the reference signal in the frequency domain. The IFFT algorithm is, then, applied. Before the received and reference signals are processed by the FFT, both the real data are converted to complex data consisting of inphase (I) and quadrature (Q) components using the Hilbert-Transform.

For estimating the Doppler velocity of a raindrop, the successive data after the pulse compression in the same range bin is processed by the FFT. In this observation, the pulse repetition frequency is about 2.0 kHz and the number of pulses of FFT is 128. The resolution of Doppler velocity is 0.15 m/s in this configuration.

C. Range Resolution

The ideal range resolution, Δr, of the radar using pulse compression can be written as

$$\Delta r = c/2B$$

where c is the speed of light, and the range resolution of our radar with bandwidth of 80 MHz is about 1.9 m. However the range sidelobe is −13 dB down from the peak. Therefore, we use the output waveform of the signal source (AWG) which is the chirp signal multiplied by the Blackman-Harris or raised-cosine window function. As a result, the range sidelobe is suppressed to −125 dB (Blackman-Harris) and −16 dB(raised-cosine), respectively. However, the mainlobe width becomes broad and the range resolution degrades to about 4 m. This result was confirmed by a

scattering experiment using the radar for a few metal plates as targets.

CALIBRATION AND EXPERIMENT CONFIGURATION

Most of the data discussed in this document were obtained at the campus of Osaka Prefecture University, Sakai, Japan with the broad band radar (BBR) in vertical pointing mode. Therefore, the radar measured the time series of the radar reflectivity profile with high space and time resolution. Table I gives the operation characteristics of our radar. Two second resolution data is obtained from the incoherent integration of 64 successive pulses and a 1-second resolution data is obtained from the incoherent integration of 128 successive pulses.

An initial observation was conducted in 2005. A micro rain radar (MRR) which is a vertical pointing FMCW radar at 24 GHz in 50 mW, was also installed 5 m away from the BBR as a reference. The MRR was operated at the resolution of 35 m in height and 60 s in time. We also used a Joss-Waldvogel disdrometer (JWD) instrument (Distromet Inc. RD-80) for the calibration and comparison of the reflectivity above ground. The disdrometer estimates rain drop size distribution (DSD) and rain rate from the vertical momentum of an impacting raindrop. The results of the rainfall observation and the comparison with the equivalent radar reflectivity factor Ze are provided by the disdrometer. Our radar was calibrated by using metal plates having known radar cross section values. The results showed that the measured and calculated radar cross section values agreed within ± 1 dB. This shows that our radar is well calibrated and stable for observing fixed targets. However, Ulbrich and Lee[1999] and Ulbrich and Miller[2001] showed, by comparing the measured Z-value with a calculated Z-value by using the disdrometer, that even a well-calibrated radar like WSR-88D has a systematic offset error in rain observations. Gage et al. [2004] showed that the serial reflectivity measurements from a disdrometer can be a good calibration for a wind profiler. Thus the calibration of the precipitation radar by the disdrometer is useful to remove the systematic offset error. In this study, we used a similar method to calibrate our radar system. Figure 2 shows scatter plots of the radar reflectivity factor of the BBR, Zm, and Ze calculated from the disdrometer. In the calculation of Ze, the Mie scattering of spherical particles is assumed. The radar reflectivity factor Ze is calculated from the DSD accumulated over each minute by the JWD. The radar data used here for comparison are the reflectivities observed at the lowest usable height of about 60 m above ground. The attenuation coefficient (dB/km) is about $0.042R1.13$ for 16 GHz [6]. As the range between radar and rain scattering volume is 40 m, the effect of attenuation is negligibly small. It can be seen that they agree well from 10 up to 50 dBZ. The minimum detectable reflectivity is about 5 dBZ. The correlation coefficient is 0.98. The root mean square difference between the BBR and the disdrometer observation is about 1.6 dBZ. The causes of the difference of 1.6 dBZ will be the differences of the location of the observed raindrops and of the rain scattering volume and so on.

We will continue efforts to minimize the calibration difference in the future. The time

series of Zm for every two-second values and Ze for every one-minute values are shown in Fig. 3. This figure shows that the BBR and the disdrometer have almost the same reflectivites.

ANALYSIS OF REFLECTIVITY PROFILE

An example of the time height cross section of the reflectivities observed simultaneously by the BBR and the MRR are shown in Fig. 4. The rain rate calculated from the disdrometer is also shown in the same temporal axis in Fig. 4. This event includes convective type rainfall exceeding more than 80 mm/h at 18:38, and no bright band is observed. Although there are several differences between the MRR and the BBR in terms of frequency, power, modulation, and data processing, the overall patterns of reflectivity profiles between the BBR and the MRR look similar except from 18:38 to 18:40 above 600 m, during which a strong rain attenuation effect is observed at the MRR. The attenuation coefficients of the MRR and the BBR are about 12 dB/km and about 4.8 dB/km for a rain rate of 80 mm/h, respectively. For example, reflectivities of the MRR and the BBR at 18:36:00 and 595 m are 37.4 and 45.9 dBZ, respectively. The attenuation values estimated by the rain rate at the surface are about 14.2 dB and 5.7 dB, respectively, and thus the corrected reflectivities of the MRR and the BBR are about the same, i.e., 52 dB.

It is clearly shown that the observations by the BBR reveal the rain structure in much more detail than the MRR, and this small-scale structure tends to be obscured in the MRR observations, indicating that the BBR observations are well suited for fine-scale measurements of rainfall at low altitude. An increase in the rainfall is similarly seen from 18:40 to 18:45 in the lower layer from the BBR and the MRR observations. Similarly, this may be largely attributable to the rainfall attenuation. However, it is difficult to correct the attenuation y rainfall in general, and if a part of it is not due to rainfall atenuation, it would be found that it strengthens toward the ground as discussed in Palmer et al. [2005].

Another example of the BBR measurement is shown in Fig. 5 for the stratiform type rain on January 14, 2006. In this 75-minute observation, many tilted rain echoes are observed. Although the horizontal distribution of precipitation cannot be seen in this vertical pointing observation, it is possible to make some speculations. If we assume no vertical wind velocity and no horizontal advection of precipitation systems, the tilted rain echo would be due to the descent of raindrops toward the ground. From the slope estimation of the tilted echoes, the terminal velocity of rain echo can be estimated. For example, the relatively strong tilted echo at 09:44 has fallen from 2000 m in height to the ground over about 130 s, giving a fall velocity of about 15 m/s. This terminal velocity can also be estimated by the Doppler spectrum measurements. Figure 6 shows the Doppler spectrum at 09:43 calculated from the phase change of 128 successive pulses. Below the melting layer at 2000 m, the maximum Doppler velocity is distributed from 4 to 8 m/s which is not consistent with the slope estimation of 15 m/s. The classical estimation assumes no horizontal advection and no vertical

wind velocity, and the rain event analyzed is a stratiform rain event which does not have a strong updraft or downdraft wind. It is possible that the apparent terminal velocity of 15 m/s from the classical estimation would be due to the advection of tilted rain streaks in the stratiform rain system.

As is clearly seen in Fig. 5 on January 14, 2006, the bright band appeared during the observation. High-resolution radar measurement is very suitable for researching the bright band. One of the Doppler spectrums of echoes between 0 and 2000 m altitude measured by the BBR at 9:43 on January 14, 2006 is shown in Fig. 6. This shows the most common profile of the bright band in this event in terms of reflectivities and Doppler spectrum. As is well known, the reflectivity profileclearly shows the V shape signature which is associated with the melting process. Just above the bright band, the reflectivity increases rapidly with decreasing height, and in the lower part of the melting layer, the reflectivity drops off sharply where the rain particles collapse to form small raindrops.

V. CONCLUSIONS

In this study, we developed a broad band radar (BBR), and an initial experiment was conducted in Osaka, Japan for studying the small-scale variability of rainfall at low altitude. The BBR uses a low-power (100 mW) 80-MHz broad band signal for transmitting with arbitrary modulation and digital pulse compression technique for detecting targets. The radar system can observe the backscattered signal from rain volume with high resolution from near the ground. The range resolution was of the order of four meters with onesecond temporal resolution. Calibration was successfully done within 1.62 dBZ using the DSD measured by the JWD, and the correlation coefficient between the radar reflectivity factor observed at 40 m above ground and calculated from the DSD was 0.98.

Two case studies were presented here, demonstrating the BBR performances. In the first case, a fine-scale measurement by the BBR was shown in contrast with the conventional radar system for a convective type event and the attenuation effect was discussed in the comparison of the MRR and the BBR. In the second case, a stratiform type rain event was analyzed. The rain streaks were clearly observed by the BBR system, and a classical estimation of rainfall velocity using the slope of the rain streaks showed a disagreement with a Doppler spectrum estimation, which suggests the existence of advection. A bright band of the stratiform rain type was observed. A vertical radar reflectivity profile and Doppler profile of rain with a bright band were observed. In these case studies, the radar was operated in the vertically pointing mode. The system can rotate and make 3 dimensional observations. This radar will be useful for studying the inhomogeneity observed in rain. It would be worth adding polarization capabilities to this radar for measuring the distribution of rain drop size. This function can be installed now, and the results of using this function will be examined in another paper.

ACKNOWLEDGEMENT

This work was supported by the Strategic Information and Communications R&D Promotion Program (SCOPE) in the Ministry of Internal Affairs and Communications. This work was also supported by the fund of CREST (Core Research for Evolutional Science and Technology) of Japan Science and Technology Agency. The authors thank Mr. H. Hanado, Dr. K. Nakagawa, and Dr. T. Iguchi for their lending the equipment necessary to pursue this research.

References

K. S. Gage, W. L. Clark, and C. R.Williams, "Determining reflectivity measurement error from serial measurements using paired disdrometers and profilers," *Geophysical Research Letters*, vol. 31, p. L23107, 2004.

R. Meneghini and T. Kozu, *Spaceborne Weather Radar*. Artech House, 1990.

R. D. Palmer, B. L. Cheong, M. W. Hoffman, S. J. Frasier, and F. J. L. Dekker, "Observations of the small-scale variability of precipitation using an imaging radar," *J. Atmos. Oceanic Technol.*, vol. 22, pp. 1122–1137, 2005.

C. W. Ulbrich and L. G. Lee, "Rainfall measurement error by WSR-88D radars due to variations in Z-R law parameters and the radar constant," *J. Atmos. Oceanic Technol.*, vol. 16, pp. 1017–1024, 1999.

C. W. Ulbrich and N. E. Miller, "Experimental test of the effects of z-r law variations on comparison of WSR-88D rainfall amounts with surface rain gauge and disdrometer data," *Weather and Forecasting*, vol. 16, pp. 369–374, 2001.

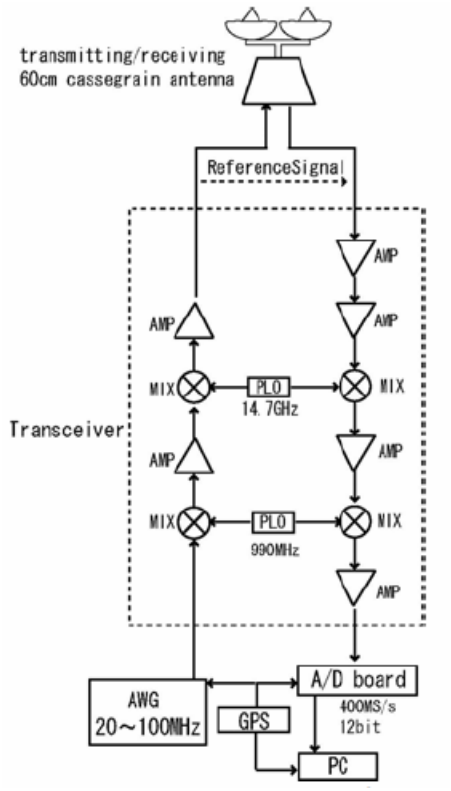

Figure 1 Schematic diagram of the radar system.

Table 1 Operating characteristics

Pulse width(τ)	128 μs (typical)
Pulse repetition time	300 or 488 μs (typical)
Time resolution	1 or 2 sec. (typical)
Number of pulses (N)	64, 128 (typical)
Transmitted frequency	15.75 GHz ± 40 MHz
Bandwidth (B)	80 MHz
Transmitted power	100 mW
Beamwidth of antennas	2 degrees
Gain of antenna	32 dB

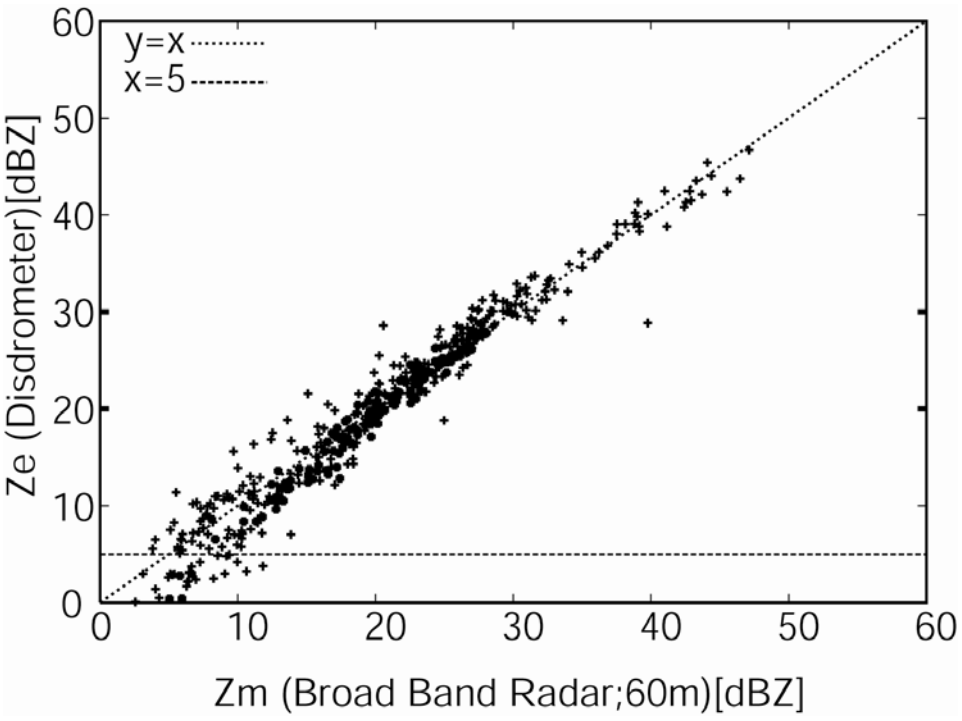

Figure 3 Scatter plot of Zm from the broad band radar and Ze from the disdrometer. The dashed line represents a 1:1 slope.

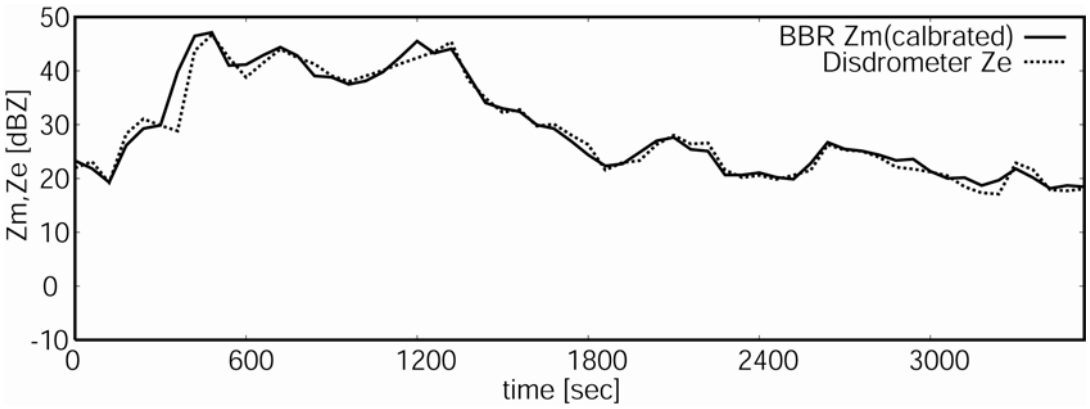

Figure 4 Time series of Zm for every 2-second, and Ze for every 1-minute mean values.

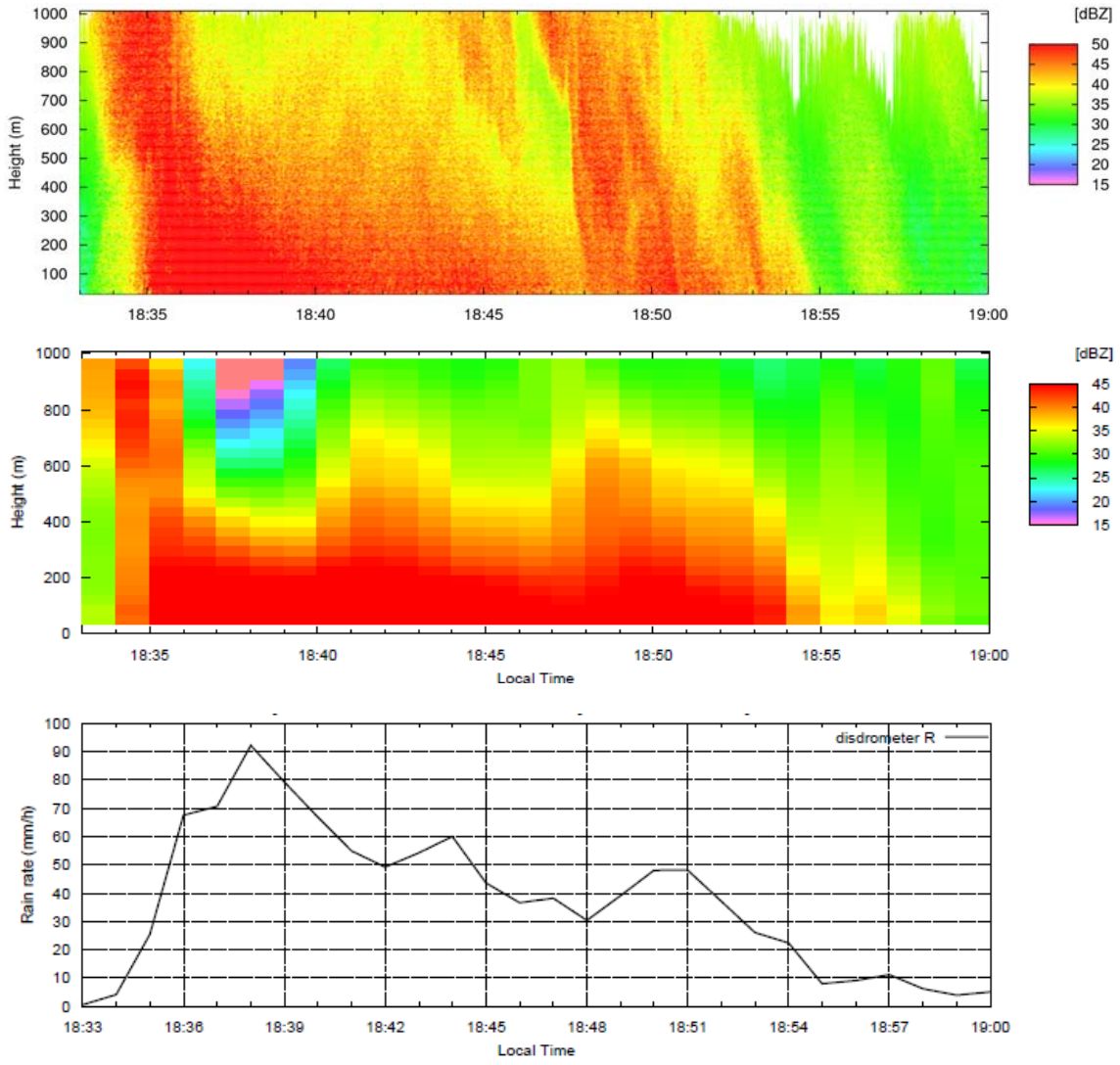

Figure 4. Time height cross section of radar reflectivities observed by the Broad band radar (upper

panel) and Micro Rain Radar (middle panel). Surface rain rate dy disdrometer is also shown in the bottom panel with same time axis.

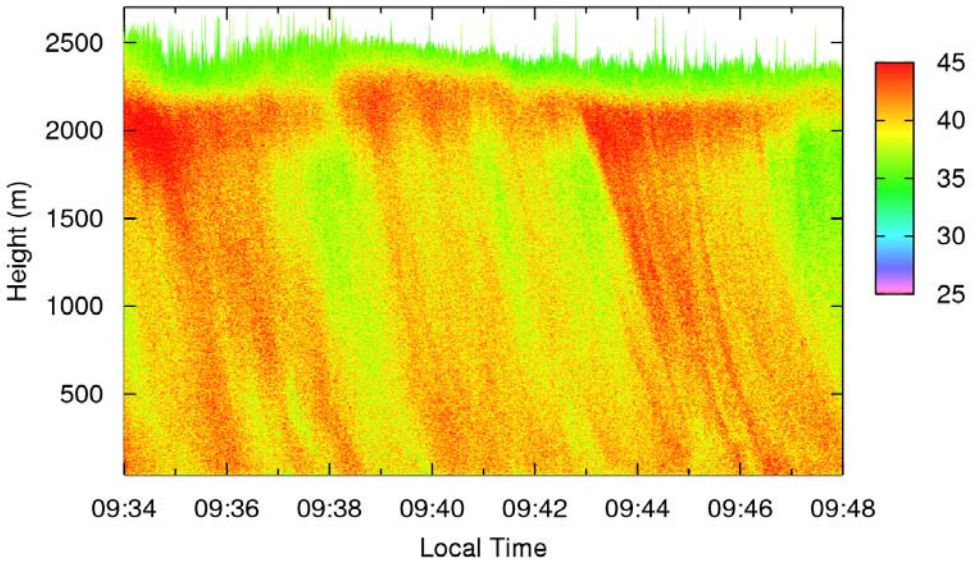

Fig.5 The BBR observation for the staratiform type rain event.

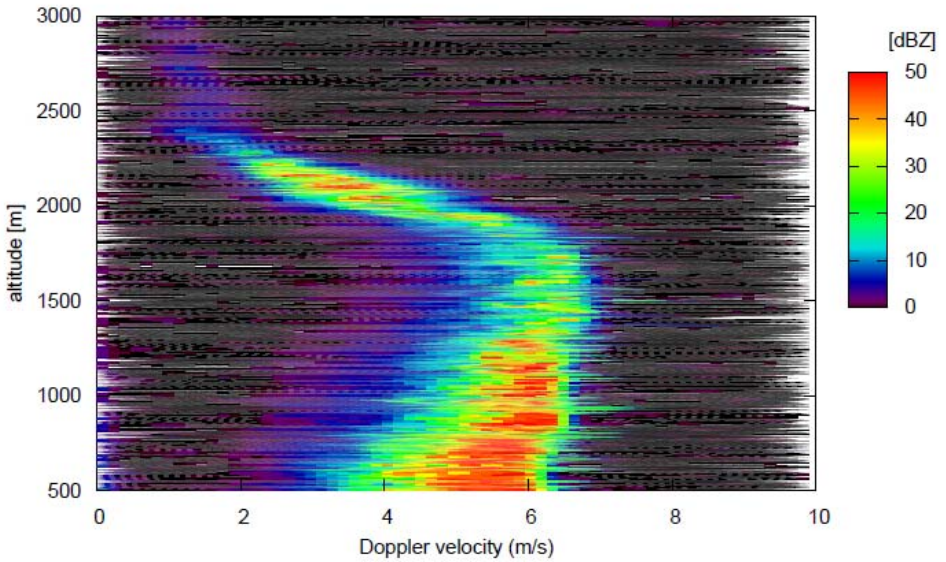

Fig. 6. Doppler spectrum